





The origin of the Perseus-arm gap revealed with VLBI astrometry

Nobuyuki Sakai¹, Hiroyuki Nakanishi², Kohei Kurahara³,
Daisuke Sakai^{3,4}, Kazuya Hachisuka³, Jeong-Sook Kim⁵ and
Osamu Kameya^{3,6}

¹National Astronomical Research Institute of Thailand (Public Organization).
email: nobuyuki@narit.or.th

²Graduate School of Science and Engineering, Kagoshima University

³National Astronomical Observatory of Japan, Oshu-shi, Iwate 023-0861, Japan

⁴The Iwate Nippo Co., Ltd.

⁵Ulsan National Institute of Science and Technology / Chungbuk National University

⁶Oshu Space & Astronomy Museum

Abstract. The Perseus arm has a gap in Galactic longitudes (l) between 50° and 80° where the arm has little star formation activity. To understand the gap, we conducted VERA (VLBI Exploration of Radio Astrometry) astrometry and analyzed archival H I data. We report on parallax and proper motion results from four star-forming regions, of which G050.2800.39 and G070.33+01.59 are associated with the gap. Perseus-arm sources G049.41+00.32 and G050.2800.39 lag relative to a Galactic rotation by 77 ± 17 km s⁻¹ and 31 ± 10 km s⁻¹, respectively. The noncircular motion of G049.41+00.32 cannot be explained by the gravitational potential of the arm. We discovered rectangular holes with integrated brightness temperatures less than 30 K arcdeg in l vs. V_{LSR} of the H I data. Also, we found extended H I emission on one side of the Galactic plane when integrating the H I data over the velocity range covering the hole. G049.41+00.32 and G050.2800.39 are moving toward the emission. The Galactic H I disk at the same velocity range showed an arc structure, indicating that the disk was pushed from the lower side of the disk. All the observational results might be explained by a cloud collision with the Galactic disk.

Keywords. Galaxy:disk, Galaxy:kinematics and dynamics, masers, instrumentation:interferometers, parallaxes

1. Introduction

The Perseus arm is one of the two (e.g., [Drimmel 2000](#); [Churchwell et al. 2009](#)) or four (e.g., [Georgelin & Georgelin 1976](#); [Russeil 2003](#)) main arms of the Milky Way, based on radio, infrared and optical observations. Using the precise locations of very young objects, [Xu et al. \(2023\)](#) revealed that the inner part of the Milky Way shows a two-arm symmetry (the Norma and Perseus arms) and the two arms extend to the outer part where there are several long irregular arms (the Centaurus, Sagittarius, Carina, Outer, and Local arms). However, the Perseus arm shows a “gap structure” in the Galactic-longitude range between $l = \sim 50^\circ$ and $\sim 80^\circ$ where the molecular line emission of CO (J=1-0) is faint compared to the other part of the arm ([Zhang et al. 2013](#)). The same tendency has been confirmed in distributions of Massive Young Stellar Objects (MYSOs) via the MSX source survey of [Urquhart et al. 2014](#)) and molecular cores (via 1.1-mm dust continuum data by [Shirley et al. 2013](#)).

We aim to understand physical mechanisms of the creation of the Perseus-arm gap based on VLBI astrometry observations. The observations combined with spectroscopic data allow us to reveal the accurate location and 3D motion of the gap structure via measurements of trigonometric parallaxes, proper motion components, and line-of-sight velocities.

2. Observations

Based on the position-velocity (i.e., Galactic longitude l vs. LSR velocity V_{LSR}) diagram of CO (Dame *et al.* 2001), we selected four MYSOs which are associated with the Perseus-arm gap. Using VERA (VLBI Exploration of Radio Astrometry), we conducted 39-epochs VLBI astrometry for 22 GHz H₂O maser emissions from the four MYSOs between the December of 2015 and the June of 2020.

The observing system of VERA including VLBI back-end system is summarized in (Oyama *et al.* 2016). Left-handed circular polarization data were recorded at 1,024 Mbps or 2 Gbps with 2-bit quantization and were correlated with Mizusawa software correlator[†]. A frequency spacing of 15.625 or 31.25 kHz was applied for 22 GHz H₂O masers, which corresponds to a velocity spacing of 0.21 or 0.42 km s⁻¹.

3. Data reduction

Data reduction was performed with the Astronomical Image Processing System (AIPS; van Moorsel *et al.* 1996). Basic amplitude and phase calibrations were applied for the data by referring to previous VERA astrometry papers (e.g., figure 11 of Kurayama *et al.* 2011).

Obtained masers' positions relative to a background continuum source were modeled using the following equations (see Kamezaki *et al.* 2012 for details):

$$\Delta\alpha\cos\delta = \pi(-\sin\alpha\cos\lambda_{\odot} + \cos\epsilon\cos\alpha\sin\lambda_{\odot}) + (\mu_{\alpha}\cos\delta)t + \alpha_0\cos\delta, \quad (1)$$

$$\Delta\delta = \pi(\sin\epsilon\cos\delta\sin\lambda_{\odot} - \cos\alpha\sin\delta\cos\lambda_{\odot} - \cos\epsilon\sin\alpha\sin\delta\sin\lambda_{\odot}) + \mu_{\delta}t + \delta_0 \quad (2)$$

where $(\Delta\alpha\cos\delta, \Delta\delta)$ are the displacements of the observed maser spot, π the trigonometric parallax, (α, δ) are the right ascension and declination of the source, λ_{\odot} is the ecliptic longitude of the Sun, ϵ is the obliquity of the ecliptic, $(\mu_{\alpha}\cos\delta, \mu_{\delta})$ are proper motion components in right ascension and declination directions, respectively, and $(\alpha_0\cos\delta, \delta_0)$ are right ascension and declination when $t = 0$.

4. Results and Discussions

4.1. New parallax and proper-motion results

We obtained new parallax and proper motion results for four MYSOs (see Table 1), of which G070.33+01.59 shows a fractional parallax error of 50%. Although the distance estimation via the parallax result of G070.33+01.59 is biased due to the large error (see Bailer-Jones 2015), we succeeded to estimate a source distance of 7.7 ± 1.0 kpc based on the measured proper motion and the LSR velocity determined by a molecular line observation. The above distance is called “2D kinematic distance”, which is less affected by noncircular motion (i.e., peculiar motion) compared to the conventional 1D kinematic distance based on the LSR velocity and a model of Galactic rotation curve. In Table 1, spiral-arm assignments of the four MYSOs are conducted using the Bayesian distance calculator[‡] of Reid *et al.* (2016) where previous parallax results are used as prior information. Also, we input the information of measured proper motions into the calculator. As a result, G050.28–00.39 and G070.33+01.59 are classified in the Perseus arm.

[†] <https://www.miz.nao.ac.jp/veraserver/system/fxcorr-e.html>

[‡] <http://bessel.vlbi-astrometry.org/node/378>

Table 1. New parallax and proper motion results.

| Target | Parallax (π) (mas) | Distance (kpc) | $\mu_\alpha \cos\delta$ (mas yr ⁻¹) | μ_δ (mas yr ⁻¹) | V_{LSR} (km s ⁻¹) | Spiral arm | Ref. |
|---------------|-----------------------------|-------------------------------------|--|---|------------------------------------|---------------|------|
| G050.28-00.39 | 0.140±0.018 | 7.1 ^{+1.1} _{-0.8} | -3.29±0.56 | -5.52±0.37 | 17±3 | Perseus | a |
| G053.14+00.07 | 0.726±0.038 | 1.4±0.1 | -1.27±1.08 | -7.15±1.07 | 22±4 | – | a |
| G070.33+01.59 | 0.074±0.037* | – | -2.82±0.29 | -4.68±0.28 | -23±5 | Perseus | b |
| G079.08+01.33 | 0.118±0.035 | 8.5 ^{+3.6} _{-1.9} | -2.49±0.14 | -3.36±0.24 | -64±1 [†] | Outer | c |

Column 1: 22 GHz H₂O maser source; Columns 2-3: parallax and corresponding distance; Columns 4-5: proper motion components in right ascension and declination directions, respectively; Column 6: LSR velocity; Column 7: The spiral-arm assignment based on the Bayesian distance calculator of Reid et al. (2016). The symbol hyphen, –, indicates *unknown* result; Column 8: the reference of the LSR velocity estimated from a molecular line observation.

References: (a) Shirley et al. (2013); (b) Anglada et al. (1996); (c) Miville-Deschênes et al. (2017).

*Since the fractional parallax error is 50%, distance estimation by simply inverting the parallax results in a significant bias (see Bailer-Jones 2015).

[†]Different LSR velocities $V_{LSR} = -18 \pm 5$ km s⁻¹ (Yang et al. 2002) and -64 ± 1 km s⁻¹ have been assigned for the source based on ¹²CO (J=1–0) observations. The latter LSR velocity is applied in this paper.

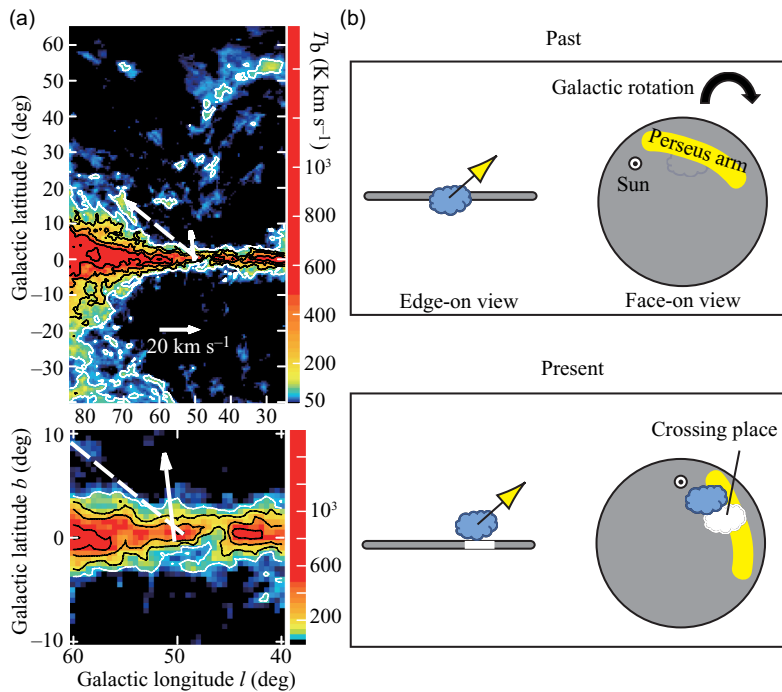


Figure 1. (a) Referring to Sakai et al. (2022). Galactic longitude vs. latitude of H I, obtained by integrating the LAB data (Kalberla et al. 2005) over the range of LSR velocity [−25, −5] km s⁻¹. The color shows the integrated brightness temperature of the H I emission. Arrows display noncircular motions of MYSOs G049.41+00.32 and G050.28–00.39. Both the sources are associated with an end-point of the Perseus-arm gap (at Galactic longitude ~50°). Bottom panel is an enlarged view of top panel. (b) Cartoon proposing a scenario how the Perseus-arm gap is created. Top panel indicates that the Galactic disk was pushed from the negative Galactic latitude side previously (i.e., a cloud collision with the Galactic disk) while bottom shows the current picture of the Milky Way reflecting observational results of H I and VLBI astrometry results.

4.2. A possible physical mechanism on the creation of the Perseus-arm gap

Using the new and previous VLBI astrometry results of the Perseus arm, we discuss kinematics especially for the noncircular motion of the arm. As shown by Fig. 4

of Sakai *et al.* (2022), the maximum and systematic noncircular motion of the arm is confirmed at an end-point of the Perseus-arm gap (at Galactic longitude $l \sim 50^\circ$; see white arrows in Fig. 1). Especially, one MYSO G049.41+00.32 lags relative to a universal rotation curve of (Reid *et al.* 2019; i.e., A5 model) by $77 \pm 17 \text{ km s}^{-1}$. Such a large noncircular motion cannot be explained by the gravitational potential of a spiral arm (e.g., see Sakai *et al.* 2019).

Figure 1 shows LAB H I data (Kalberla *et al.* 2005) integrated over the LSR velocity range $[-25, -5] \text{ km s}^{-1}$ covering the LSR velocity of G049.41+00.32, $-21 \pm 1 \text{ km s}^{-1}$ (Svoboda *et al.* 2016). The figure indicates the existence of H I stream above the Galactic plane (at $b > 0^\circ$). The H I mass of the stream is $\sim 8 \times 10^6 M_\odot$ (solar mass) at the distance of G049.41+00.32, $7.6_{-1.4}^{+2.3} \text{ kpc}$ (Reid *et al.* 2019). Also, we can see arc-shape structure in the Galactic disk, which is offset by $\sim 0.4^\circ$ from G049.41+00.32.

To explain all the observational results as well as the physical origin of the Perseus-arm gap, we propose a cloud collision with the Galactic disk (see the cartoon of Fig. 1). To confirm the hypothesis, further studies should be conducted in the future (e.g., the distance and metallicity of the H I stream; the time of a cloud collision).

References

- Anglada, G., Estalella, R., Pastor, J., Rodriguez, L. F., & Haschick, A. D. 1996, *ApJ*, 463, 205
- Bailer-Jones, C. A. L. 2015, *PASP*, 127, 994
- Churchwell, E., Babler, B. L., Maede, M. R., *et al.* 2009, *PASP*, 121, 213
- Dame, T. M., Hartmann, D., & Thaddeus, P. 2001, *ApJ*, 547, 792
- Drimmel, R. 2000, *A&A*, 358, L13
- Georgelin, Y.-M., & Georgelin, Y.-P. 1976, *A&A*, 49, 57
- Kalberla, P. M. W., Burton, W. B., Hartmann, D., Arnal, E. M., Bajaja, E., Morras, R., & Pöppel, W. G. L. 2005, *A&A*, 440, 775
- Kamezaki, T., Nakagawa, A., Omodaka, T., *et al.* 2012, *PASJ*, 64, 7
- Kurayama, T., Nakagawa, A., Sawada-Satoh, S., Sato, K., Honma, M., Sunada, K., Hirota, T., & Imai, H. 2011, *PASJ*, 63, 513
- Miville-Deschênes, M. -A., Murray, N., & Lee, E. J. 2017, *ApJ*, 834, 57
- Oyama, T., Kono, Y., Suzuki, S., *et al.* 2016, *PASJ*, 68, 105
- Reid, M. J., Dame, T. M., Menten, K. M., & Brunthaler, A. 2016, *ApJ*, 823, 77
- Reid, M. J., *et al.* 2019, *ApJ*, 885, 131
- Russeil, D. 2003, *A&A*, 397, 133
- Sakai, N., Reid, M. J., Menten, K. M., Brunthaler, A., Dame, T. 2019, *ApJ*, 876, 30
- Sakai, N., Nakanishi, H., Kurahara, K., Sakai, D., Hachisuka, K., Kim, J. -S., & Kameya, O. 2022, *PASJ*, 74, 209
- Shirley, Y. L., Ellsworth-Bowers, T. P., Svoboda, B., *et al.* 2013, *ApJS*, 209, 2
- Svoboda, B. E., *et al.* 2016, *ApJ*, 822, 59
- Urquhart, J. S., *et al.* 2007, *A&A*, 474, 891
- Urquhart, J. S., Figura, C. C., Moore, T. J., *et al.* 2014, *MNRAS*, 437, 1791
- van Moorsel, G., Kembell, A., & Greisen, E. 1996, in ASP Conf. Ser., 101, Astronomical Data Analysis Software and Systems V, ed. G. H. Jacoby & J. Barnes (San Francisco: ASP), 37
- Xu, Y., Hao, C. J., Liu, D. J., *et al.* 2023, *ApJ*, 947, 54
- Yang, J., Jiang, Z., Wang, M., Ju, B., & Wang, H. 2002, *ApJS*, 141, 157
- Zhang, B., Reid, M. J., Menten, K. M., *et al.* 2013, *ApJ*, 775, 79